

UDC 548.736.15:621.794.4

**L. M. Yang, J. H. Gong\*, Z. M. Yue, S. N. Liu, Q. L. Chen,  
J. Gao\*\***

School of Mechanical, Electrical and Information Engineering,  
Shandong University, Weihai, China

\*gongjh@sdu.edu.cn

\*\*shdgj@sdu.edu.cn

### **Preferential etching by flowing oxygen on the {100} surfaces of HPHT single-crystal diamond**

*Application of diamond is determined by its oxidation behaviour in some measure. Oxidation process of single-crystal diamond prepared under high pressure and high temperature has been studied by the thermal analysis, scanning electron microscope and Raman spectrometer. The result of a simultaneous thermal analysis indicates that single-crystal diamond is oxidized at ~ 818 °C at a heating rate of 5°C/min in the flowing oxygen. Based on the data of the thermal analysis at different heating rates, the activation energy is calculated by the Kissinger method. A weight loss rate increases with the rising heat treatment temperature from 600 to 800°C. After the oxidation at 800 °C, etch pits emerge on the {100} surfaces of single-crystal diamond, while the {111} surfaces are smooth. Shapes of the etch pits on the {100} surfaces are inverted pyramidal hollows, with edges direction parallel to the <110> direction.*

**Keywords:** single-crystal diamond, preferential etching, oxidation, thermal stability.

#### **INTRODUCTION**

Due to its greatest hardness, diamond is usually used as an abrasive powder or cutting tool material [1]. Diamond is chemically stable at room temperature, but when temperature is above 700 °C, diamond becomes metastable and inclined to be damaged [2]. Poor thermal stability limits the application of diamond due to the temperature increase, specially during the polishing or cutting process.

It is of a vital importance to investigate the oxidation behavior of diamond. Some studies including experiments and simulations have been done to investigate the oxidation process and reveal the oxidation mechanism of diamond. For instance, heated in air in the temperature range of 27–1227 °C, diamond will be oxidized at around 477 °C and the {111} surfaces are preferentially oxidized compared with {100} surfaces [3]. Hyperthermal atomic oxygen can cause a partial graphitization on the {111} surfaces of chemical vapor deposited (CVD) diamond and etch pits will emerge on the {111} surfaces, but hyperthermal atomic oxygen collisions with the {100} surfaces will only result in elastic scattering without etching [4]. When oxygen collides with the {100} plane, a nearly full ketone coverage will form and protect the {100} surfaces from further erosion [5]. There are more boundaries and defects on the {111} surfaces. During a thermal oxidation, the

{111} facets are selectively removed and single-crystal diamond microneedles can be obtained as a result [6]. Aerobic oxidation can also remove the graphitic and amorphous carbon in nano-diamond, meanwhile increasing the proportion of  $sp^3$ -hybridized carbon [7]. Moreover, based on the selective oxidation, diamond electrode can be selectively etched, thereby obtaining a large surface area [8].

As is well known, high pressure and high temperature (HPHT) and CVD are two mainstream methods to synthesize diamond [9]. According to the previous researches, the {111} surfaces are going to be selectively etched during aerobic oxidation. But most works are about CVD diamond films. Few articles present the oxidation process of single-crystal diamond synthesized under HPHT, not to mention its oxidation mechanism.

The activation energy is an important parameter to describe the minimum energy which must be available to result in a chemical reaction. There are several ways to calculate the apparent activation energy [10] and the Kissinger method is a practical one [11]. Using this method, people can compare thermal stabilities of diamond prepared under different conditions.

In this work, series of experiments are carried out to study the oxidation process of single-crystal diamond. Simultaneous thermal analyses are conducted to reveal the thermal resistance of single-crystal diamond. Activation energy of a single-crystal is calculated based on the data of thermal analysis. Scanning electronic microscope (SEM) and Raman spectrometer are used to investigate the morphology of surfaces and C–C structure inside single-crystal diamond, respectively.

## EXPERIMENTAL

### Synthesis of single-crystal diamond

Using graphite as the carbon source and Fe–Ni–Co alloy powders as a catalyst, single-crystal diamonds were prepared in a cubic anvil HP-HT apparatus, with pressure of  $\sim 5.0$ – $6.0$  GPa and temperature of  $\sim 1500$ – $1800$  °C.

### TG-DSC analysis

The as-prepared diamond was divided into 2 categories both for anisothermally thermal gravimetric (TG) and differential scanning calorimetry (DSC) analysis. Starting weight of diamond in the two categories was  $35 \pm 5$  mg and  $20.5 \pm 1.5$  mg, respectively. In the first category, to study the influence of oxygen on diamond at different temperatures, single-crystal diamond was separated into 3 groups and heated up from 30 to 600, 700 and 800 °C at 30 °C/min in a 50 mL/min flowing oxygen, respectively, then cooled down directly. After TG and DSC analysis, the residual material of each group was collected for further characterization. The residual material was taken out when furnace temperature was lower than 50 °C. In the second category, single-crystal diamond was heated up from 30 to 1200 °C at 5, 10, 20 and 40 °C/min in a 50 mL/min flowing oxygen for calculating the activation energy, respectively. Because of the high temperature, diamond would react with oxygen and no more residual diamond material would be found after the thermal analysis. All the experimental materials in the 2 categories were put into  $Al_2O_3$  crucible and analyzed in a simultaneous thermal analyzer made by Mettler Toledo. The thermal experimental data was displayed in a STARE Evaluation Software and exported to other graphing software.

### Morphology and C–C bond characterization

A Nova NanoSEM 450 with 5.00 kV scanning voltages was used to observe the oxidized and original surface of single-crystal diamond. A Renishaw inVia Laser

Raman spectroscopy with a 532 nm laser beam for excitation and spectral repeatability of  $\pm 0.2 \text{ cm}^{-1}$  was used to reveal the C–C bonds of single-crystal diamond.

## RESULTS AND DISCUSSIONS

### Thermal analysis of single-crystal diamond

The weight of the pristine and thermally treated diamonds at 600, 700 and 800 °C in flowing oxygen, as well as the weight loss rate of single-crystal diamond are shown in the table. After 600–800 °C thermal treatment in flowing oxygen, mass of the diamond changes little, which means that a complete oxidation reaction does not take place. But the weight loss rate increases with the increasing oxidative temperature. This indicates that a high temperature with oxygen does have influence on single-crystal diamond. The higher the temperature is, the severer oxidation happens.

### Weight loss of diamond before and after thermal treatment

Temperature, °C	Weight		Weight loss rate, %
	before oxidation	after oxidation	
600	33.8400	33.8130	0.080
700	37.6120	37.5626	0.131
800	30.6300	30.2453	1.256

Figure 1 shows the TG-DSC curves of single-crystal diamond heating from 30 to 1200 °C at 5 °C/min. A TG curve reveals that the weight of diamond decreases dramatically at 818.06 °C, which is the onset of the oxidation temperature. Exothermic peak in DSC curve appearing from 818.32 °C is in good accordance with the TG result.

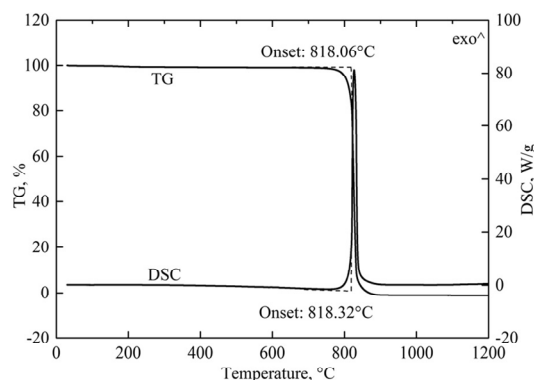


Fig. 1. TG-DSC curves of single-crystal diamond heated from 30 to 1200 °C at 5 °C/min in flowing oxygen.

Figure 2, *a* summarizes the DSC curves of single-crystal diamond heating from 30 to 1200 °C at 5, 10, 20 and 40 °C/min, respectively. The onset temperatures of exothermic peak at different heating rates can be obtained with the help of STARE Evaluation Software. As is shown in Fig. 2, *a*, peak temperatures  $T_p$  are 826.92, 869.00, 885.15 and 909.25 °C, corresponding to the heating rates: 5, 10, 20 and 40 °C/min, respectively.

The Kissinger method is a powerful tool to determine the activation energy [11]. A remarkable advantage of the Kissinger method is that it can be used to calculate activation energy regardless of the reaction order of the system [12]. Based upon this method, the obtained activation energy is a sum of a chemical reaction and physical process. Therefore, it is also called apparent activation energy [13]. The Kissinger method can be expressed as an equation:

$$\frac{d\left(\ln\frac{\beta}{T_p^2}\right)}{d\left(\frac{1}{T_p}\right)} = -\frac{E}{R},$$

where  $\beta$  is the heating rate,  $T_p$  is the maximum peak temperature,  $R$  is the gas constant and  $E$  is the activation energy. In current experiment, maximum peak temperatures at different heating rates can be obtained from Fig. 2, *a*. In DSC curves, peaks corresponding to larger heating rates will shift toward higher temperatures due to a thermal inertia. A linear relationship between  $\ln(\beta/T_p^2)$  and  $1/T_p$  is drawn in Fig. 2, *b* and the gas constant  $R$  is known (8.314 J/(mol·K)). Finally, the activation energy of 253.87 KJ/mol is obtained, which is consistent with the previous study [14]. It is worth noting that during the calculation of the activation energy, the unit of the temperature is converted to Kelvin (K).

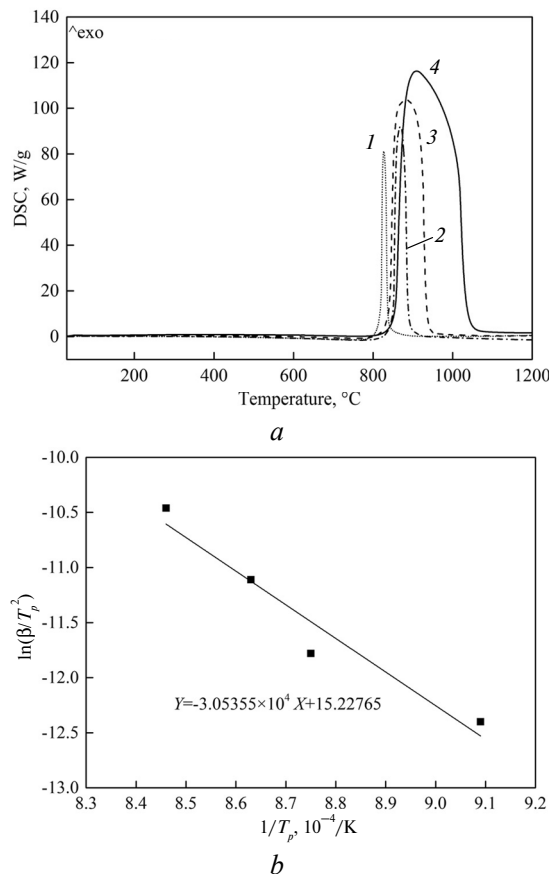


Fig. 2. DSC curves of single-crystal diamonds heated from 30 to 1200 °C at 5 (1), 10 (2), 20 (3) and 40 (4) °C/min, respectively (*a*); linear relationship between  $1/T_p$  and  $\ln(\beta/T_p^2)$  (*b*).

### Morphology of single-crystal diamond

Figure 3, *a* shows the morphology of the pristine single-crystal diamond in a cubic-octahedron shape. From Fig. 3, *a*, it is found that the single-crystal diamond is mainly composed of the  $\{100\}$  and  $\{111\}$  surfaces, with a small number of high index  $\{311\}$  surfaces. These high index  $\{311\}$  surfaces are supposed to improve the adhesive ability of a single-crystal diamond when diamond is used in diamond tools [15]. The  $\{111\}$  surfaces are smooth and flat, while the  $\{100\}$  and  $\{311\}$  surfaces seem rough. There are some lamellar patterns covering these surfaces, as indicated in dashed-line rectangles in Fig. 3, *a* and enlarged in Fig. 3, *b* and Fig. 3, *c*. These lamellar patterns are formed in connection with Fe. When Fe is used as a catalyst, Fe will dissolve the diamond surface to produce  $\text{Fe}_3\text{C}$  during quenching process, forming lamellar structures [16]. Moreover, the aerobic oxidation after 600 and 700 °C does not change the morphologies of single-crystal diamond apparently, but an interesting phenomenon is observed after the aerobic oxidation at 800 °C.

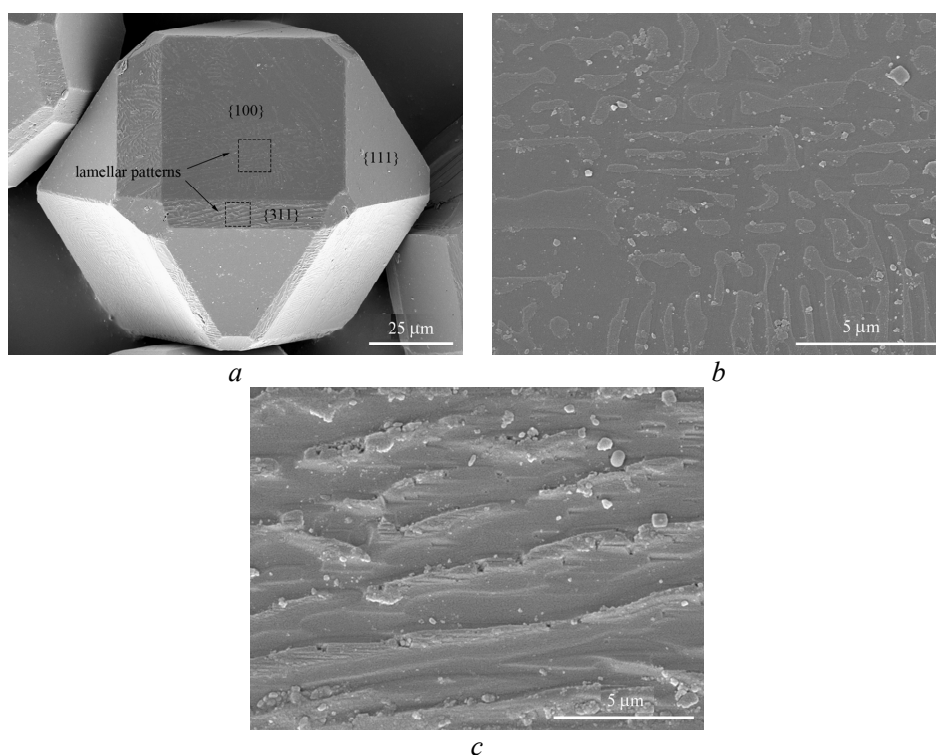


Fig. 3. Morphology of single-crystal diamond before thermal oxidation (*a*); enlarged view of lamellar patterns on the  $\{100\}$  surface (*b*) and enlarged view of lamellar patterns on the  $\{311\}$  surface (*c*).

As is shown in Fig. 4, *a*, numerous etch pits form on the  $\{100\}$  surfaces while the  $\{111\}$  surfaces keep smooth except the irregular large pits emerged on the upper  $\{111\}$  surface. As indicated by the ellipse in Fig. 4, *a*, these large size pits are supposed to originate from the growing process and expanded during the oxidation process. After the oxidation process, a  $\{311\}$  surface seems rough, but with no etch pits too. Shapes of etch pits on the  $\{100\}$  surfaces are inverted pyramidal hollows, with edge directions parallel to the  $\langle 110 \rangle$  direction, as shown in Fig. 4, *b*, which is similar to the etch pits on the  $\{100\}$  surface by oxygen/hydrogen plasma treatment

[17]. In other words, the  $\{100\}$  surfaces are preferentially etched during thermal oxidation in flowing oxygen. Combining with changes of weight in table, it can be found that although  $800\text{ }^{\circ}\text{C}$  doesn't reach the onset oxidative temperature, the oxidation reaction still takes place on the  $\{100\}$  surfaces of some grains to a certain degree, forming etching pits. Considering there are more lamellar structures and pits on the  $\{100\}$  faces than on the  $\{111\}$  faces, the morphology of this single-crystal diamond seems reasonable, because the oxidation process occurs preferentially on grain boundaries and local defects [2]. This is different from the CVD diamond. In CVD diamond, the  $\{111\}$  faces are always preferentially etched because there are more defect on the  $\{111\}$  surfaces [3, 6]. In fact, there are more dangling bonds on the  $\{100\}$  surfaces than on the  $\{111\}$  surfaces and this is supposed to be the main reason why the  $\{100\}$  surfaces are preferentially etched.

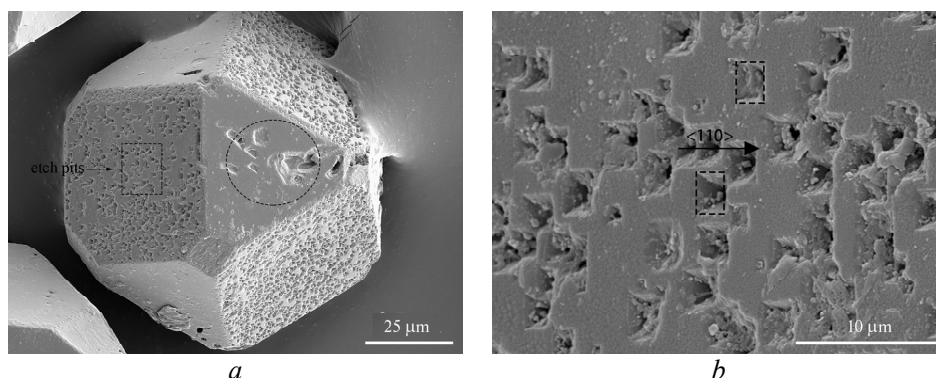


Fig. 4. Morphology of single-crystal diamond after  $800\text{ }^{\circ}\text{C}$  thermal oxidation (a), and enlarged view of etch pits on  $\{100\}$  surface (b).

### Raman spectroscopy of single-crystal diamond

Figure 5 shows the Raman scatterings of diamond before and after 600, 700 and  $800\text{ }^{\circ}\text{C}$  thermal analysis. From  $1200$  to  $1600\text{ cm}^{-1}$ , there are two main peaks locating at  $\sim 1332$  and  $\sim 1423\text{ cm}^{-1}$ . First-order scattering peak appearing at  $\sim 1332\text{ cm}^{-1}$  is the characteristic peak of a diamond phase. When all the peaks in a Raman scattering lie in a flat baseline, that kind of diamond can be thought as a comparatively pure diamond [18]. And obviously, current tested diamond are composed of impurities more or less. Especially at  $\sim 1423\text{ cm}^{-1}$ , an obvious peak occurs. That can be assigned to transpolyacetylene [19] or amorphous carbon [20]. Whatever, the phase represented by the  $1423\text{ cm}^{-1}$  peak must be some non-diamond phase. Moreover, the intensity of the  $1423\text{ cm}^{-1}$  peak seems to increase when it is  $700\text{ }^{\circ}\text{C}$ , then decrease when the temperature is  $800\text{ }^{\circ}\text{C}$ . When the oxidation temperature is  $800\text{ }^{\circ}\text{C}$ , the peak at  $1423\text{ cm}^{-1}$  nearly disappears and the Raman line around  $1423\text{ cm}^{-1}$  is almost flat. This phenomenon is in connection with the reduction of impurities or the increase of  $\text{sp}^3$  hybridization of carbon [6, 7].

### CONCLUSION

In this paper, series of simultaneous thermal analyses are conducted on HPHT single-crystal diamond to reveal its oxidation process. In the flowing oxygen at a heating rate of  $5\text{ }^{\circ}\text{C}/\text{min}$ , the oxidation process of single-crystal diamond starts at  $\sim 818\text{ }^{\circ}\text{C}$ . Meanwhile, based on the data of the thermal analysis at different heating rates, the activation energy of  $253.87\text{ KJ/mol}$  is obtained by the Kissinger method. A weight loss rate increases with the temperature rising from  $600$  to  $800\text{ }^{\circ}\text{C}$ . After

the heat treatment at 800 °C in the flowing oxygen, early stage of oxidation etching occurs. The {100} surfaces of single-crystal diamond are preferentially etched by a flowing oxygen and numerous etch pits emerge. The shapes of etch pits are inverted pyramidal hollows, with edge directions parallel to  $\langle 110 \rangle$ . However, the flowing oxygen doesn't etch the {111} surfaces and the morphology of the {111} surfaces keep smooth. The reason for different etching results between the {100} and {111} surfaces is supposed to be the more dangling bonds existing on the {100} surfaces than on the {111} surfaces.

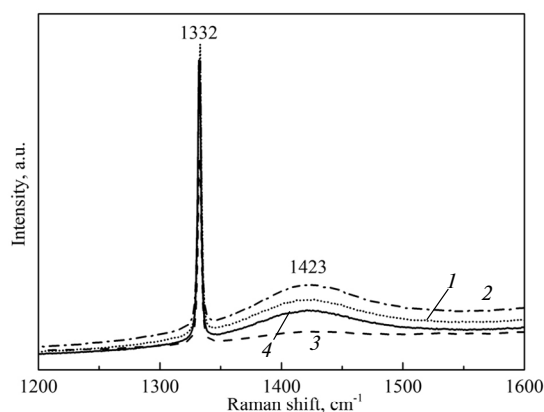


Fig. 5. Raman spectroscopy of single-crystal diamond treated at different temperatures: 600 (1), 700 (2), 800 (3) °C, untreated (4).

This work was supported by the Natural Science Foundation of Shandong Province (No. ZR2014EMM011) and National Natural Science Foundation of China (No. 51272139).

*Застосування алмазу в якійсь мірі визначається його поведінкою при окисленні. За допомогою термічного аналізу, скануючої електронної мікроскопії і спектроскопії комбінаційного розсіювання світла вивчено процес окислення монокристалічного алмазу, отриманого при високому тиску і високій температурі. Одночасний термічний аналіз показав, що монокристалічний алмаз окислюється при  $\sim 818$  °C при швидкості нагріву  $5$  °C/хв в потоці кисню. На основі даних термічного аналізу при різних швидкостях нагрівання розраховано енергію активації за методом Кіссінджера. Швидкість втрати ваги зростає з підвищенням температури термообробки від  $600$  до  $800$  °C. Після окислення при температурі  $800$  °C ямки травлення з'являються на поверхні {100} монокристалічного алмазу, в той час як поверхні {111} гладкі. Форма ямок на поверхнях {100} – перевернуті пірамідальні западини з ребрами в напрямку паралельному  $\langle 110 \rangle$ .*

**Ключові слова:** монокристалічний алмаз, вибіркве травлення, окислення, термічна стабільність.

*Применение алмаза в какой-то мере определяется его поведением при окислении. С помощью термического анализа, сканирующей электронной микроскопии и спектроскопии комбинационного рассеяния света изучен процесс окисления монокристаллического алмаза, полученного при высоком давлении и высокой температуре. Одновременный термический анализ показывает, что монокристаллический алмаз окисляется при  $\sim 818$  °C при скорости нагрева  $5$  °C/мин в потоке кислорода. На основе данных термического анализа при различных скоростях нагрева рассчитана энергия активации по методу Киссинджера. Скорость потери веса возрастает с повышением температуры термообработки от  $600$  до  $800$  °C. После окисления при температуре  $800$  °C ямки травления появляются на поверхности {100} монокристаллического алмаза, в то время как*

поверхности  $\{111\}$  гладкие. Форма ямок на поверхностях  $\{100\}$  – перевернутые пирамидальные впадины с ребрами в направлении параллельном  $\langle 110 \rangle$ .

**Ключевые слова:** монокристаллический алмаз, избирательное травление, окисления, термическая стабильность.

1. Eberle G., Dold C., Wegener K. Laser fabrication of diamond micro-cutting tool-related geometries using a high-numerical aperture micro-scanning system // *Int. J. Adv. Manuf. Tech.* – 2015. – **81**, N 5. – P. 1117–1125.
2. Pu J. C., Wang S. F., Sung J. C. High-temperature oxidation behaviors of CVD diamond films // *Appl. Surf. Sci.* – 2009. – **256**, N 3. – P. 668–673.
3. Sun C. Q., Xie H., Zhang W. *et al.* Preferential oxidation of diamond  $\{111\}$  // *J. Phys. D: Appl. Phys.* – 2000. – **33**, N 17. – P. 2196–2199.
4. Shpilman Z., Gouzman I., Grossman E. *et al.* Oxidation and etching of CVD diamond by thermal and hyperthermal atomic oxygen // *J. Phys. Chem. C.* – 2010. – **114**, N 44. – P. 18996–19003.
5. Paci J. T., Schatz G. C., Minton T. K. Theoretical studies of the erosion of (100) and (111) diamond surfaces by hyperthermal O(3P) // *J. Phys. Chem. C.* – 2011. – **115**, N 30. – P. 4770–14777.
6. Zolotukhin A. A., Dolganov M. A., Alekseev A. M., Obratsov A. N. Single-crystal diamond microneedles shaped at growth stage // *Diam. Relat. Mater.* – 2014. – **42**. – P. 15–20.
7. Wolcott A., Schiros T., Trusheim M. E. *et al.* Surface structure of aerobically oxidized diamond nanocrystals // *J. Phys. Chem. C.* – 2014. – **118**, N 46. – P. 26695–26702.
8. Zhang J., Nakai T., Uno M. *et al.* Effect of the boron content on the steam activation of boron-doped diamond electrodes // *Carbon.* – 2013. – **65**. – P. 206–213.
9. Hu M. H., Bi N., Li S. S. *et al.* Studies on synthesis and growth mechanism of high quality sheet cubic diamond crystals under high pressure and high temperature conditions // *Int. J. Refract. Met. Hard. Mater.* – 2015. – **48**. – P. 61–64.
10. Starink M. J. The determination of activation energy from linear heating rate experiments: a comparison of the accuracy of isoconversion methods // *Thermochim. Acta.* – 2003. – **404**, N 1. – P. 163–176.
11. Kissinger H. E. Reaction kinetics in differential thermal analysis // *Anal. Chem.* – 1957. – **29**, N 11. – P. 1702–1706.
12. Malow M., Krause U. The overall activation energy of the exothermic reactions of thermally unstable materials // *J. Loss Prevent. Proc.* – 2004. – **17**, N 1. – P. 51–58.
13. Rocco J. A. F. F., Lima J. E. S., Frutuoso A. G. *et al.* Thermal degradation of a composite solid propellant examined by DSC // *J. Therm. Anal. Calorim.* – 2004. – **75**, N 2. – P. 551–557.
14. De Theije F. K., Roy O., van der Laag N. J., van Enckevort W. Oxidative etching of diamond // *Diam. Relat. Mater.* – 2000. – **9**, N 3. – P. 929–934.
15. Zhang Z. F., Jia X. P., Liu X. B. *et al.* Effects of aluminum additive on diamond crystallization in the Fe–Ni–C system under high temperature and high pressure conditions // *Sci. China Phys. Mech.* – 2012. – **55**, N 5. – P. 781–785.
16. Kanda H., Akaishi M., Setaka N. *et al.* Surface structures of synthetic diamonds // *J. Mater. Sci.* – 1980. – **15**, N 11. – P. 2743–2748.
17. Tsubouchi N., Mokuno Y., Shikata S. Characterizations of etch pits formed on single crystal diamond surface using oxygen/hydrogen plasma surface treatment // *Diam. Relat. Mater.* – 2015. – **63**. – P. 43–46.
18. Praver S., Nemanich R. J. Raman spectroscopy of diamond and doped diamond // *Philos. T. R. Soc. A.* – 2004. – **362**, N 1824. – P. 2537–2565.
19. Ferrari A. C., Robertson J. Origin of the  $1150\text{ cm}^{-1}$  Raman mode in nanocrystalline diamond // *Phys. Rev. B.* – 2001. – **63**, N 12, art. 121405.
20. Thomsen C., Reich S. Double resonant Raman scattering in graphite // *Phys. Rev. Lett.* – 2000. – **85**, N 24. – P. 5214–5217.

Received 23.11.15